Received 11 January 2021; revised 22 February 2021; accepted 21 March 2021.
Date of publication 29 March 2021; date of current version 8 April 2021.

Digital Object Identifier 10.1109/OJCOMS.2021.3068866

Performance Analysis of Intelligent Reflecting Surface-Assisted Wireless System With Non-Ideal Transceiver

MOHD HAMZA NAIM SHAIKH (Graduate Student Member, IEEE), VIVEK ASHOK BOHARA (Senior Member, IEEE), ANAND SRIVASTAVA, AND GOURAB GHATAK (Member, IEEE)

Wirocomm Research Group, Department of Electronics and Communication Engineering, Indraprastha Institute of Information Technology Delhi, New Delhi 110020, India

CORRESPONDING AUTHOR: M. H. N. SHAIKH (e-mail: hamzan@iiitd.ac.in)

This work was supported by the Visvesvaraya Ph.D. Scheme for Electronics and IT by Ministry of Electronics and Information Technology, Government of India, being implemented by the Digital India Corporation.

ABSTRACT Intelligent Reflecting Surfaces (IRSs) have recently emerged as a promising solution for realizing the smart radio environment concept by leveraging the characteristics of metamaterials and large antenna arrays. However, the existing works on IRS do not account for the transceiver impairments while analyzing the performance of IRS assisted wireless systems. This paper investigates the impact of transceiver hardware imperfections on the performance of IRS-assisted wireless systems. Specifically, we have analyzed the spectral efficiency (SE), the energy efficiency (EE) and the outage probability of IRS-assisted wireless systems by deriving their closed-form expressions and verifying them through simulation results. The results show the importance of modeling and compensating for hardware impairment as they significantly restrict the performance of such systems.

INDEX TERMS Intelligent reflecting surfaces, performance analysis, spectral efficiency, energy efficiency, outage, hardware impairments, relay.

I. INTRODUCTION

HIGH throughput and high energy efficiency are the two key requirements for modern communication systems. The ever increasing demand for high throughput is fueled by ubiquitous mobile services with enhanced quality-of-service (QoS). Further, the innovative applications such as augmented and virtual reality, unmanned mobility, big data analytics, three-dimensional (3D) media, e-health, etc., are highly data intensive [1], [2]. A major characteristic of the futuristic wireless network is the propensity to support such massive traffic. Thus, it requires a very large area spectral efficiency (hundreds of bits/s/Hz/sq. km) and ultra high throughput per user equipment (multiple Gbps) [1]. A scaling of 1000-times in the system capacity has been envisioned in the current wireless system [3]. This explosion of wireless data has continuously driven the advancement in wireless technologies such as millimeter-wave (mmWave) communication, large-scale multiple-input multiple-output (MIMO), capacity-achieving turbo and polar codes. These technologies have also been advocated for the fifth-generation (5G) wireless standard [4]. For further enhancement of data rate, the combination of mmWave with massive MIMO has also been proposed. However, the deployment of large-scale MIMO usually results in a high cost of implementation and increased power consumption. However, the combination of mmWave and massive MIMO needs sophisticated signal processing techniques, which require expensive and energy consuming hardware [5].

Along with high spectral efficiency (SE), the emerging and futuristic wireless networks (5G and beyond) have also raised concerns on the consumption of energy while operating these wireless networks. Further, it is also anticipated

that the future wireless network will have to connect over a hundred billion devices in a dense deployment, which includes base stations and access points [6]. Consequently, the bits/Joule energy efficiency (EE) has also emerged as a key performance metric that ensures the sustainability of wireless networks [7], [8]. A recent survey on the implementation of energy efficient wireless networks has recommended multiple joint approaches to limit the overall energy consumption [9]. A few of the prescribed approaches are the usage of renewable energy along with employing energy-efficient hardware, optimal resource allocation, and deployment based on reducing energy consumption. Moreover, deploying a massive number of antennas results in a substantial improvement in the EE of the wireless system, as shown in [10], [11].

Recently, intelligent reflecting surfaces (IRSs) has been proposed as a potential innovative solution to achieve both the goals, i.e., high EE and high SE [5], [12]. IRS has also been acknowledged as one of the critical enablers technology for the sixth-generation (6G) wireless network [13], [14]. IRS is specifically a re-configurable array of passive reflecting elements, wherein each of the elements can independently alter the phase and/or attenuation of the incident signal. Cumulatively, the reflected signal is altered as such that the desired channel response can be realized through proper phase shifting at each of the reflecting elements. The reflected signal can be combined constructively from all the paths to enhance the received signal power or can be combined destructively to mitigate the undesired interference, thus improving the overall performance of the wireless system [15]. The individual unit of IRS can be implemented through reflect-arrays which employ a varactor diode or a PIN diode, where the resonating frequency of these diodes can be controlled electronically [16], [17]. Further, with the advent of Micro-Electrical-Mechanical Systems (MEMS) and eta materials, a real-time reconfiguration of the phase shifts of IRS has also been demonstrated. This real-time reconfiguration of IRS phase-shift has widely enhanced its applicability for deployment across various wireless networks [18]. Moreover, the low hardware footprint of IRS structure facilitates the wider deployment across the different urban structures in the outdoor environment such as buildings, factory ceilings, roof-tops, etc. Consequently, IRS can easily be integrated into the existing wireless communication environment [19].

Contrary to the conventional relaying, the beamforming gain in the IRS is achieved through intelligent reflection and without consuming any additional energy for re-transmission. IRS simply reflects the incoming signal by suitably adjusting the phase of the reflected signal from each of the reflecting elements in order to have a constructive combination of the signal at the desired receiver. Additionally, the IRS does not require any dedicated time/frequency resource for the re-transmission of the incoming signal. Since IRS does not employ a power amplifier, the circuit power consumption is much less than that in a regular amplify-and-forward (AF) relay [20]. Thus, from an energy consumption standpoint, the IRS is far more energy-efficient as compared to conventional relaying [21].

A. RELATED WORK

In [22], the authors have investigated the approximate achievable data rate assuming that the channels between a transmitter to IRS and IRS to the receiver are independent and Rician distributed. In [23], authors have analyzed the asymptotic uplink sum-rate of a IRS-assisted system in the Rician channel. IRS is adopted for downlink communication in the multi-user scenario for enhancing the EE in [20]. Specifically, in [20], the authors have reported a 300% increase in the EE of IRS vis-a-vis traditional AF relaying based resource allocation. Similarly, the authors in [19], [20], [24] considered the IRS for assisting downlink transmission scenario for multiple users and worked on maximizing the sum-rate. Further, in [21] and [25], the authors have derived the upper-bound for the error performance of IRS-assisted wireless systems. It can be noted that these upper-bound are quite tight for IRS with a large number of reflecting elements; however, the lower bound is not quite accurate when the number of reflecting elements is small. Further, in [26], authors have provided bit error rate (BER) analysis for IRS-assisted non-orthogonal multiple access (NOMA) systems. However, the authors employed the central limit theorem (CLT) to characterize the distribution of the equivalent channel; the results are precise for IRS having a large number of reflecting elements.

In [27], IRS has been employed in simultaneous wireless information and power transfer (SWIPT) aided system, where the energy harvesting is enhanced by the IRS. Further, a self-sustainable IRS have been proposed for a wireless powered communication network (WPCN), where IRS improves downlink energy transfer and uplink information transmission for multiple users [28]. Similarly, in [29], IRS has been proposed to the realm of index modulation (IM), where the author has proposed IRS-space shift keying (SSK) and IRS-spatial modulation (SM) schemes for future wireless communication systems. The joint passive and active beamforming at IRS has been studied in [30] for obtaining the average received power at the user. IRS has also been explored for physical layer security (PLS) in [31]. Lastly, [32] employs IRS for vehicular communications, where the IRS enhances the link-performance of both the vehicle-to-vehicle and vehicle-to-infrastructure link. The seminal work of Renzo *et al.* comprehensively discussed the concept and state-of-art research for IRSs [33]. Further, it also presented the communication-theoretic framework based on electromagnetic theory for modeling, analysis, optimization and deployment of futuristic IRS empowered smart radio environment. In addition, the work of [15], [17], [21], [34] presented a comprehensive review of IRS empowered communication.

Some recent works have also analyzed the trade-offs of IRS vis-a-vis conventional relaying. For instance,

TABLE 1. Related work.

Reference	Work	Contribution
Huang et al. [20]	Energy Efficiency	Energy-efficient design by optimizing the transmit power and phase shift for downlink transmission
Zhang et al. [22]	Optimal Phase	Analytically evaluated the optimal number of required bit for discrete phase shift at IRS
Jung et al. [23]	Uplink Sum Rate	Asymptotic analysis of uplink sum-rate distribution
Basar et al. [21] and [25]	SER	Upper bound on the SER in IRS-assisted wireless system
Thirumavalavan et al. [26]	IRS-assisted NOMA	BER analysis of IRS-assisted NOMA transmission
Pan et al. [27]	SWIPT with IRS	IRS aided MIMO broadcasting where the energy harvesting capabilities of SWIPT are enhanced by IRS
Bjornson et al. [33]	IRS v/s DF Relaying	Compared the energy-efficiency and required transmit power for both IRS and DF Relaying
Renzo et al. [34]	IRS v/s Relaying	Discussed the key differences and similarities between IRS and relaying
Boulogeorgos et al. [35]	IRS v/s AF Relaying	Analytical Performance Evaluation and Comparison of IRS and AF Relaying
Boulogeorgos et al. [36]	Impact of Hardware Impairments	Analyzed the impact of non-ideal hardware on outage, diversity and provided the upper bound on spectral efficiency

Bjornson *et al.* have compared the EE performance of IRS-assisted systems against decode-and-forward (DF) relaying assuming the channel to be deterministic [35], while, Renzo *et al.* discussed the key differences and similarities between IRSs and the relays in [36]. The authors have provided different set of simulations in order to compare the data rate of IRS-assisted system with the relays. Further, in [37] IRS-assisted systems were compared with relay in terms of outage probability, symbol-error rate (SER) as well as ergodic capacity while assuming that the transceivers in both IRS-assisted wireless system and relay-assisted wireless systems were equipped with ideal RF front-ends.

It is evident from above, there is a dearth of literature on the performance of IRS-assisted wireless systems in the presence of non-ideal transceiver hardware, as most of the prior work assume ideal hardware scenario, and thus overlooking the impact caused by the impairment due to non-ideal hardware. In [38], authors have studied the impact of transceiver hardware imperfection in a IRS-assisted system. However, the study was limited in terms of outage probability and upper bound of the SE. The ergodic SE has not been analyzed in [38], further, the authors have also not considered the EE of the system.

B. MOTIVATION AND CONTRIBUTIONS

Inspired by the current research in IRS, in this paper, we investigate the impact of hardware impairments on the performance of a IRS-assisted wireless system. The major contributions of the proposed work can be summarized as follows:

- In this work, we present a model to characterize the impact of transceiver impairments on IRS-assisted wireless systems taking into account the effect of channel fading as well as the size of IRS. The size is characterized by the number of reflecting elements (REs), M, in the IRS.
- Next, we derive the closed-form expressions for the outage probability and SE of the IRS-assisted wireless systems by first obtaining the instantaneous signal-to-distortion-plus-noise-ratio (SDNR) and then utilizing it to derive the above expressions.
- In continuation of the above, we also present the SE analysis for three special cases, viz. a) single reflecting element based IRS i.e., $M = 1$, b) very large sized IRS, i.e., $M >> 1$ and c) high SNR approximation.
- Finally, we present the analytical evaluation of EE for the IRS-assisted wireless system. The results reveal that in the for an IRS-assisted wireless system, the EE reduces with increasing the number of reflecting elements.

From the derived analytical and simulation results, it has been shown that the hardware impairments severely restrict the performance of IRS-assisted wireless system. Unlike the conventional IRS system wherein the gain due to IRS increases with the number of REs, the SE saturates with increasing the number of REs due to hardware impairments. Specifically, after saturation, no further gain can be achieved in the SE by increasing the number of REs in the IRS. A similar observation has been made while increasing transmit power. Further, it has also been shown that the EE further decreases by increasing the number of reflecting elements. This is due to the fact that increasing the number of reflecting elements raises power consumption, consequently decreasing the overall EE.

Moreover, the result also shows that nonlinear HPA is the major source of distortion. The distortion due to HPA saturates the SE, which consequently degrades the EE of the IRS-assisted system. The impact of nonlinearity can be mitigated by operating the HPA in back-off, thus improving the SE and the outage performance. However, increasing the IBO reduces the efficiency of HPA, which results into reduction in the overall EE of the IRS-assisted system. In comparison to [38], the proposed work provides a complete analytical framework to analyze the EE performance of IRS-assisted systems while considering the impact of hardware impairment. Furthermore, we have also derived the closed-form

TABLE 2. List of acronyms.

Abbreviation	Description
AF	Amplify-and-Forward
AM/AM	Amplitude-to-Amplitude
AM/PM	Amplitude-to-Phase
AWGN	Additive White Gaussian Noise
BER	Bit Error Rate
CDF	Cumulative distribution function
CLT	Central limit theorem
DF	Decode-and-Forward
EE	Energy Efficiency
EVM	Error Vector Magnitude
HPA	High Power Amplifier
IBO	Input Back-Off
IM	Index Modulation
IRS	Intelligent Reflecting Surface
LO	Local Oscillator
MEMS	Micro-Electrical-Mechanical Systems
MIMO	Multiple-Input and Multiple-Output
NOMA	Non-Orthogonal Multiple Access
OFDM	Orthogonal Frequency Division Multiplexing
PDF	Probability Density Function
PLS	Physical Layer Security
QoS	Quality-of-Service
RE	Reflecting Element
RF	Radio Frequency
RV	Random Variable
SDNR	Signal-to-Distortion plus Noise Ratio
SE	Spectral Efficiency
SER	Symbol Error Rate
SM	Spatial Modulation
SNR	Signal-to-Noise Ratio
SSPA	Solid State Power Amplifier
SWIPT	Simultaneous Wireless Information and Power Transfer
WPCN	Wireless Powered Communication Network
5G	Fifth-Generation
6G	Sixth-Generation

TABLE 3. Notations.

Symbol	Definition
$\Pr[\cdot]$	Probability
$\mathrm{E}[\cdot]$	Expectation operator
$\mathrm{tr}[\cdot]$	Trace operator
$[\cdot]^{\mathrm{H}}$	Hermitian operator
$\mathrm{E}_i(\cdot)$	The Exponential integral
${}_2F_1(\cdot,\cdot;\cdot;\cdot)$	The Gauss hyper-geometric function
$\Gamma(\cdot)$	Gamma function
$\gamma(\cdot,\cdot)$	Lower incomplete Gamma function
$K_v(.)$	Modified Bessel function (second kind, order v)
$F_0(.)$	Polygamma function (zero order)
$G_{\cdot,\cdot}^{\cdot,\cdot}\left(\cdot \mid \begin{matrix}\cdot,\cdot\\ \cdot,\cdot\end{matrix}\right)$	Meijer's G function
$f_{\mathcal{G}}(x)$, $F_{\mathcal{G}}(x)$	The PDF and CDF of random variable $\mathcal{G}$

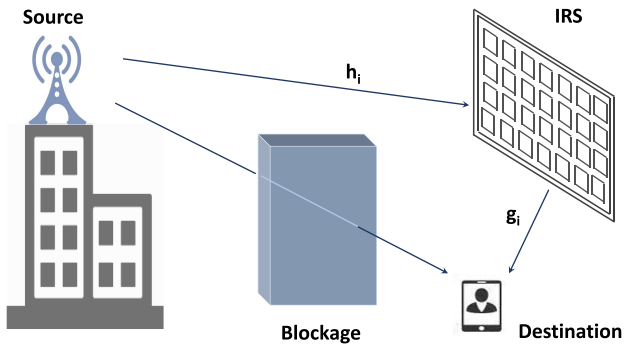

FIGURE 1. Schematic for the IRS-Assisted Wireless System.

expressions for the SE of the aforementioned system. At the end, the efficacy of the analytical derivations has been validated through simulations. To the best of our knowledge, this work is the first to theoretically investigate the EE performance of the IRS-assisted system impaired with a non-ideal transceiver.

C. ORGANIZATION AND NOTATIONS

The organization of this paper is as follows: Section II provides an overview of the IRS-assisted wireless system, description of transceiver hardware impairments and behavior modeling of HPA. Section III derives the closed-form expressions for SE, EE and outage. The simulation results are presented in Section IV and finally, Section V concludes this paper. Additionally, for convenience, we list the abbreviations used in Table 2.

The major notations used in this paper are as follows: The bold lower and upper cases represent vectors and matrices respectively (e.g., $\mathbf{x}$ and $\mathbf{X}$). Complex Gaussian distribution is represented with $\mathcal{CN}(\mu, \sigma^2)$, where μ is the mean and σ^2 denotes the variance. The remaining of the notations are summarized in Table 3.

II. SYSTEM MODEL

As shown in Fig. 1, we consider a scenario in which a source node (S) communicates with a destination node (D) via IRS. The IRS comprises of M number of reflecting elements (REs). Further, it is assumed that the direct link between the source and destination is not available due to a blockage. The fading channel between the source and the ith RE is denoted by h_i, whereas g_i is the channel between the ith RE and the destination. Both h_i and g_i are assumed to be independent and identically distributed (i.i.d). and follow the Rayleigh distribution. The above assumptions are inline with the pre-existing works, which consider the fact that even if the line-of-sight links exist between the source and IRS and/or IRS and destination are blocked, there still exist extensive scatterers [20]–[22], [37].

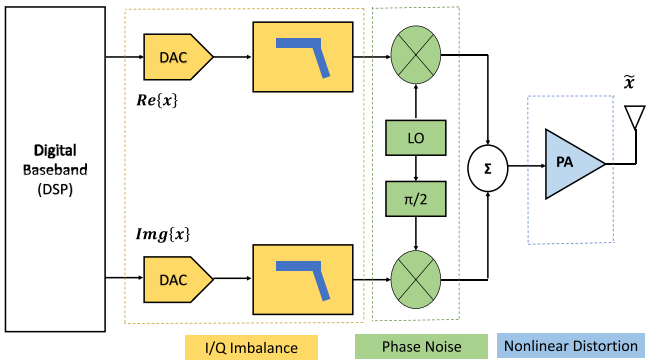

FIGURE 2. Schematic showing various imperfections at the source transceiver.

A. TRANSCEIVER IMPAIRMENTS

In this subsection, we discuss the non-idealities in the transceiver hardware that causes the signal distortion. The general assumption of ideal hardware is not realistic as the transceiver architecture at the source and destination are prone to various inevitable additive impairments such as I/Q imbalance, phase noise and radio frequency (RF) nonlinearities. Infact, even in the presence of mitigation schemes applied at the transmitter and the receiver, the residual impairments lead to inevitable distortion noise. A block diagram of a typical transmitter is shown in Fig. 2. The baseband I and Q signals are up-converted to the desired RF after traversing through the modulator. An ideal local oscillator (LO) is intended to provide an exact 90 degrees phase shift between the I/Q branches along with equal gain. However, a phase imbalance occurs due to the non-idealities of the LO, where the phase shift is not exactly 90 degrees. This also results in a gain mismatch, and the combined effect of the gain and phase imbalances is referred to as I/Q imbalance. Similarly, the power amplifier (PA), which is generally the last block in the transmit chain, is a nonlinear device that results in in-band as well as out-of-band distortion. This results in the degradation of the error vector magnitude (EVM) and the spectral regrowth of the transmitted signal.

As described in the literature, these residual impairments can be characterized in terms of distortions, which can be: a) multiplicative, when the received signals are shifted in phase; b) additive, where a distortion noise is added whose variance is proportional to the power of the transmitted signal and received signal; and c) amplified thermal noise [39]. However, for the IRS-assisted wireless system, the PA will have a larger role since only a fraction of power is reflected from the IRS and reaches the receiver.

B. HIGH POWER AMPLIFIER (HPA) MODEL

As described in the literature, HPA is one of the most crucial component in the transmit RF-chain. Further, HPA is also the major source of nonlinearity in the transmit RF-chain. Since the HPAs are designed to provide maximum efficiency in the saturation region, multi-carrier wideband communication techniques, like the most widely employed orthogonal frequency division multiplexing (OFDM), are highly impacted due to clipping of the peak signal. A lot of literature has been contributed to mitigate the impact of nonlinear distortion due to HPA. Specifically, the proper modeling of HPA is the key to study the impact of nonlinear distortion and mitigating techniques. So, in this subsection, we describe the behavior modeling of the nonlinear HPA present at the source.

A nonlinear HPA is generally characterized by amplitude-to-amplitude (AM/AM) and amplitude-to-phase (AM/PM) distortion. The signal at the output of the HPA can be expressed as [40]

$$\psi = \Xi_a(\phi)\ \exp\big(j\big(\arg(\phi) + \Xi_p(\phi)\big)\big), \tag{1}$$

where, $\arg(\phi)$ is the phase of the complex input signal to HPA, ϕ, and $\Xi_a(.)$, $\Xi_p(.)$ are the AM/AM and AM/PM characteristics function respectively.

For the solid-state power amplifier (SSPA), a Rapp model[1] can be used for the behavioral characterization, where the AM/AM and AM/PM functions can be given as

$$\Xi_a(\phi) = |\phi|\left[1 + \left(\frac{|\phi|}{A_{sat}}\right)^{2\tau}\right]^{-\frac{1}{2\tau}}, \tag{2}$$

and

$$\Xi_p(\phi) = \Theta\left(\frac{|\phi|}{A_{sat}}\right)^4, \tag{3}$$

where A_{sat} is the HPA saturation amplitude, τ is the smoothness factor which regulates the transition of linear domain to the saturation domain. As τ converges to infinity, SSPA effectively converges to the soft-envelope limiter (SEL) model which is characterizes by a linear piece-wise model. Further, since Θ is typically zero as the AM/AM distortion is much more significant in SSPA [43], (1) can be re-written as

$$\psi = \frac{|\phi|\exp(j(\arg(\phi)))}{\left[1 + \left(\frac{|\phi|}{A_{sat}}\right)^{2\tau}\right]^{\frac{1}{2\tau}}}, \tag{4}$$

or equivalently

$$\psi = \phi\mathcal{F}(|\phi|), \tag{5}$$

with

$$\mathcal{F}(|\phi|) = \left[1 + \left(\frac{|\phi|}{A_{sat}}\right)^{2\tau}\right]^{-\frac{1}{2\tau}}. \tag{6}$$

Now using the Bussgang theorem [44], which states that the output of a non-linear HPA can be decomposed into two terms; (a) a linear scaling parameter, α, which provides the linear gain of the input signal and (b) a non-linear distortion

1. Although this work considers the Rapp model, the proposed analytical framework remains valid for other models as well such as polynomial, Saleh Model etc. [41], [42].

parameter, δ, uncorrelated with the input signal with $\delta \in \mathcal{CN}(0, \xi_\delta^2)$. So, in this case, (5) can be rewritten as

$$\psi = \alpha\phi + \delta. \tag{7}$$

Now, we can derive the expressions of α and ξ_δ^2 as follows.

The scaling parameter α can be derived as

$$\alpha = \frac{\mathrm{E}\left[\phi^*\psi\right]}{\mathrm{E}\left[|\phi|^2\right]}. \tag{8}$$

From [45], α can be evaluated as

$$\alpha = \frac{A_{sat}}{2\sigma_{in}}\left[\frac{2A_{sat}}{\sigma_{in}} - \sqrt{\pi}\,\mathrm{erfc}\left(\frac{A_{sat}}{\sigma_{in}}\right)\exp\left(\frac{A_{sat}^2}{\sigma_{in}^2}\right) \times \left(\frac{2A_{sat}^2}{\sigma_{in}^2} - 1\right)\right], \tag{9}$$

where erfc(.) is the complementary error function. Similarly the variance of δ can be evaluated as

$$\xi_\delta^2 = \mathrm{E}\left[|\psi|^2\right] - \alpha\mathrm{E}\left[\phi\psi^*\right]. \tag{10}$$

Now from [45], ξ_δ^2 can be expressed as

$$\xi_\delta^2 = \sigma_{in}^2\left[\frac{A_{sat}^2}{\sigma_{in}^2}\left(1 + \frac{A_{sat}^2}{\sigma_{in}^2}\exp\left(\frac{A_{sat}^2}{\sigma_{in}^2}\right)\mathrm{E}_i\left(-\frac{A_{sat}^2}{\sigma_{in}^2}\right)\right) - \alpha^2\right]. \tag{11}$$

or equivalently it can be rewritten as

$$\xi_\delta^2 = \kappa_\delta^2\sigma_{in}^2, \tag{12}$$

where κ_δ^2 represent the scaling parameter for the input signal power, σ_{in}^2.

Practically the impacts of distortion due to the HPA nonlinearity is mitigated by operating the HPA at input back-off (IBO) from the given saturation level. From the literature, the widely accepted definition of the IBO is given as

$$\mathrm{IBO} = 10\log_{10}\left(\frac{A_{sat}^2}{\sigma_{in}^2}\right). \tag{13}$$

Increasing the IBO shifts the HPA operation towards the linear region from the saturation region. Consequently, the output of HPA is linearized as the nonlinear distortion is reduced. However, it may also be noted that the HPAs are designed to provide maximum efficiency while operating in the saturation region. Thus, increasing the IBO reduces HPA efficiency; consequently, the EE of the overall system suffers.

C. SIGNAL MODEL

Consequently at the source, the above imperfections will result into a mismatch between the actual transmitted signal and the desired signal, x, where $x \in \mathcal{CN}(0, \sigma_{in}^2)$. So from (7), the actual transmitted signal, $\tilde{x}$, can be rewritten as

$$\tilde{x} = \alpha x + \delta, \tag{14}$$

At destination, the baseband equivalent received reflected signal from IRS can be obtained as

$$y = \sum_{i=1}^{M} h_i g_i r_i \tilde{x} + w_d + n, \tag{15}$$

where, n denotes the additive white Gaussian noise (AWGN) and which is modeled as a zero-mean complex Gaussian process having a variance of σ^2.

Now representing the equivalent source-to-IRS-to-destination channel by $\mathcal{G}$, (15) can be represented as

$$y = \mathcal{G} r_i \tilde{x} + w_d + n, \tag{16}$$

with

$$\mathcal{G} = \sum_{i=1}^{M} |h_i||g_i|, \tag{17}$$

where, w_d is the distortion from the receiver hardware imperfections at the destination, and can be modeled as a zero-mean complex Gaussian process[2] with variance

$$\xi_d^2 = \kappa_d^2\mathcal{G}^2\sigma_{in}^2, \tag{18}$$

where κ_d is a proportionality constant, the value of κ_d controls the level of impairment [48].

Moreover, r_i represents the response of the ith RE and it can be obtained as

$$r_i = |r_i|\exp(j\varphi_i), \tag{19}$$

where φ_i denotes the phase shift that is applied by the ith RE of the IRS.

Further, without losing generality, we assume that $|r_i| = 1$. This assumption is inline with realistic implementations, as discussed in [37]. The IRS can be configured to provide optimal phase shift,[3] assuming that the perfect channel estimates are available at IRS. Thus, the optimal phase can be adjusted as

$$\varphi_i = -\left(\varphi_{h_i} + \varphi_{g_i}\right), \tag{20}$$

so, for the optimal phase at IRS, (19) can be rewritten as

$$r_i = \exp\left(-j\left(\varphi_{h_i} + \varphi_{g_i}\right)\right). \tag{21}$$

Now by substituting (21) into (15), the received signal at the destination can be expressed as

$$y = \mathcal{G}\tilde{x} + w_d + n. \tag{22}$$

2. Please note, the Gaussian noise characterization of destination imperfection is valid since the received signal undergoes multiple transformations and thus the aggregated distortion can be modeled through Gaussian process. Not only it is an accurate characterization as this model has been validated by several analytical as well as experimental works [46]–[49], it also represent the worst-case scenario.

3. Please note that, the impact of limited phase-shift has been analyzed in [22], where the authors have proved that the required number of phase shifts decreases with the size of IRS. Specifically, the authors have shown that 3-bits are sufficient for small IRS ($M \approx 3$), 2-bits for moderate size IRS ($M \approx 300$) and 1-bit for infinitely large sized IRS ($M \approx 3 * 10^{70}$).

Thus, the baseband equivalent received signal in (22) can be rewritten by substituting (14) as

$$\begin{aligned} y &= \mathcal{G}\alpha x + \mathcal{G}\delta + w_d + n, \\ &= \mathcal{G}\alpha x + \mathcal{W} + n, \end{aligned} \tag{23}$$

where, $\mathcal{W}$ denotes aggregated distortion caused by the hardware impairments at the source and the destination.

From (23), it is evident that for a given channel realization, the aggregated impact of source and destination hardware imperfections can be modeled via a zero-mean random variable process with variance

$$\sigma_w^2 = |\mathcal{G}|^2\left(\kappa_\delta^2 + \kappa_d^2\right)\sigma_{in}^2. \tag{24}$$

Further from (24), it can be observed that increasing the transmission power increases κ_δ^2 and κ_d^2, consequently the variance of distortion noise due to hardware imperfections increases.

Now, it can also be noted here that (23) reduces to the ideal transceiver case when $\kappa_\delta = \kappa_d = 0$. A similar observation can be made for the case when the impact of hardware imperfections is neglected. Further, from (24), for both these cases $\sigma_w^2 = 0$. Similarly, as described in (13), operating the HPA with IBO reduces the impact of nonlinearity, i.e., increasing IBO reduces κ_δ^2, this corresponds to the moderately nonlinear scenario, where the nonlinearity is controlled through IBO. Thus, the current analytical framework is capable of analyzing various scenarios through appropriate selection of simulation parameter.

III. PERFORMANCE ANALYSIS

In this section, we present the theoretical analysis for the impact of hardware imperfections on the performance of IRS-assisted wireless systems. Specifically, we evaluate the instantaneous end-to-end SDNR, which is further utilized to derive the closed-form expressions for the outage probability. Further, the spectral efficiency is formulated and evaluated for different cases. Specifically, the three special cases, viz. for $M = 1$, large M and high SNR approximation, are also considered. Finally, we present the energy efficiency evaluation where the power modeling is also discussed.

From (23) and (24), the instantaneous SDNR can be obtained as

$$\rho = \frac{\alpha^2|\mathcal{G}|^2\sigma_{in}^2}{|\mathcal{G}|^2\left(\kappa_\delta^2 + \kappa_d^2\right)\sigma_{in}^2 + \sigma^2}, \tag{25}$$

or equivalently

$$\rho = \frac{\alpha^2|\mathcal{G}|^2}{\left(\kappa_\delta^2 + \kappa_d^2\right)|\mathcal{G}|^2 + \frac{1}{\rho_s}}, \tag{26}$$

where

$$\rho_s = \frac{\sigma_{in}^2}{\sigma^2}, \tag{27}$$

denotes the transmit signal-to-noise ratio (SNR).

The normalized instantaneous rate R_{in} for the source-to-destination link through IRS can be formulated as

$$\begin{aligned} R_{in} &= \log_2(1+\rho), \\ &= \log_2\left(1 + \frac{\alpha^2|\mathcal{G}|^2}{\left(\kappa_\delta^2 + \kappa_d^2\right)|\mathcal{G}|^2 + \frac{1}{\rho_s}}\right). \end{aligned} \tag{28}$$

Next, we provide the statistical characterization of the end-2-end (e2e) channel gain. The probability density function (PDF) and cumulative density function (CDF) of $\mathcal{G}$ can be respectively expressed as [37]

$$f_{\mathcal{G}}(x) = \frac{x^a}{b^{a+1}\Gamma(a+1)}\exp\left(-\frac{x}{b}\right), \tag{29}$$

and

$$F_{\mathcal{G}}(x) = \frac{\gamma\left(1+a, \frac{x}{b}\right)}{\Gamma(a+1)}, \tag{30}$$

where

$$a = \frac{k_1^2}{k_2} - 1, b = \frac{k_2}{k_1}, \tag{31}$$

with

$$k_1 = \frac{M\pi}{2}, k_2 = 4M\left(1 - \frac{\pi^2}{16}\right). \tag{32}$$

Special Case: This refers to the specific case where the IRS is just a single RE, i.e., $M = 1$. In this scenario, channel gain $\mathcal{G}$ is the product of two independent and identically random variables (RVs) with Rayleigh distribution. Thus, the PDF and CDF for this special case follows a double Rayleigh distribution which can be expressed as below [37]

$$f_{\mathcal{G}}^s(x) = zK_0(x), \tag{33}$$

and

$$F_{\mathcal{G}}^s(x) = 1 - xK_1(x), \tag{34}$$

where $K_0(.)$ and $K_1(.)$ denotes the second kind of modified Bessel functions having the order of 0 and 1 respectively.

A. OUTAGE PROBABILITY

The e2e outage from the source-to-IRS and IRS-to-destination can be defined in terms of rate threshold, R_{th}, as below:

$$P_{out} = \Pr[R_{in} < R_{th}]. \tag{35}$$

Now from (28), the outage can be formulated as:

$$P_{out} = \Pr\left[\log_2\left\{1 + \frac{\alpha^2|\mathcal{G}|^2\sigma_{in}^2}{\left(\kappa_\delta^2 + \kappa_d^2\right)|\mathcal{G}|^2\sigma_{in}^2 + \sigma^2}\right\} < R_{th}\right], \tag{36}$$

or equivalently

$$P_{out} = \Pr\left[\frac{\alpha^2|\mathcal{G}|^2}{\left(\kappa_\delta^2 + \kappa_d^2\right)|\mathcal{G}|^2 + \frac{1}{\rho_s}} < \rho_{th}\right], \tag{37}$$

where $\rho_{th} = 2^{R_{th}} - 1$ is the SNR threshold. After some mathematical manipulation, the outage probability, P_{out} can be evaluated as:

$$\begin{aligned} P_{out} &= \Pr\left[|\mathcal{G}|^2 > \frac{\alpha^2\rho_s}{\rho_{th}} - \alpha^2\rho_s\left(\kappa_\delta^2 + \kappa_d^2\right)\right], \\ &= \Pr\left[|\mathcal{G}| < \frac{1}{\sqrt{\frac{\alpha^2\rho_s}{\rho_{th}} - \alpha^2\rho_s(\kappa_\delta^2 + \kappa_d^2)}}\right], \\ &= \Pr[|\mathcal{G}| < \Upsilon], \end{aligned} \tag{38}$$

where

$$\Upsilon = \frac{1}{\sqrt{\frac{\alpha^2\rho_s}{\rho_{th}} - \alpha^2\rho_s\left(\kappa_\delta^2 + \kappa_d^2\right)}}. \tag{39}$$

Next, from (29) the outage probability, P_{out}, can be evaluated as

$$P_{out} = \int_0^{\Upsilon} f_{\mathcal{G}}(x)dx, \tag{40}$$

or, equivalently

$$P_{out} = F_{\mathcal{G}}(\Upsilon), \tag{41}$$

which can be simplified by utilizing (30) and expressed as

$$P_{out} = \frac{\gamma\left(a+1, \frac{\Upsilon}{b}\right)}{\Gamma(a+1)}. \tag{42}$$

Similarly for the special case of $M = 1$, the outage probability, P_{out}, in (41) can be evaluated by utilizing (34) as below

$$P_{out} = 1 - \Upsilon K_1(\Upsilon). \tag{43}$$

B. SPECTRAL EFFICIENCY (SE)

Now, the spectral efficiency (SE) can be defined as

$$SE = \mathbb{E}\left[\log_2(1+\rho)\right], \tag{44}$$

or equivalently

$$SE = \int_0^{\infty} \log_2(1+\rho) f_{\mathcal{G}}(x)\mathrm{dx}. \tag{45}$$

Substituting (26) into (45), the SE can be rewritten as

$$SE = \int_0^{\infty} \log_2\left\{1 + \frac{\alpha^2 t^2}{\left(\kappa_\delta^2 + \kappa_d^2\right)t^2 + \frac{1}{\rho_s}}\right\} f_{\mathcal{G}}(t)\mathrm{dt}, \tag{46}$$

Now the SE as defined in (46) can be evaluated by utilizing (29) as

$$\begin{aligned} SE = &\frac{1}{b^{a+1}\Gamma(a+1)} \\ &\times \int_0^{\infty} \log_2\left\{1 + \frac{\alpha^2 t^2}{\left(\kappa_\delta^2 + \kappa_d^2\right)t^2 + \frac{1}{\rho_s}}\right\} t^a \exp\left(-\frac{t}{b}\right)\mathrm{dt}, \end{aligned} \tag{47}$$

After some mathematical manipulation, (47) can be reformulated as

$$\begin{aligned} SE = &\frac{1}{b^{a+1}\ln(2)\Gamma(a+1)} \\ &\times \int_0^{\infty} t^a \exp\left(-\frac{t}{b}\right) \\ &\times \left\{\ln\left(1 + c_1 t^2 \rho_s\right) - \ln\left(1 + c_2 t^2 \rho_s\right)\right\}\mathrm{dt}, \end{aligned} \tag{48}$$

or equivalently

$$SE = \frac{1}{b^{a+1}\ln(2)\Gamma(a+1)}\{\mathcal{I}_1 - \mathcal{I}_2\}, \tag{49}$$

where

$$\mathcal{I}_1 = \int_0^{\infty} t^a \exp\left(-\frac{t}{b}\right)\ln\left(1 + c_1\rho_s t^2\right)\mathrm{dt} \tag{50}$$

and

$$\mathcal{I}_2 = \int_0^{\infty} t^a \exp\left(-\frac{t}{b}\right)\ln\left(1 + c_2\rho_s t^2\right)\mathrm{dt} \tag{51}$$

with

$$c_1 = \alpha^2 + \kappa_\delta^2 + \kappa_d^2, \tag{52}$$

$$c_2 = \kappa_\delta^2 + \kappa_d^2. \tag{53}$$

From [50, Ch. 3.2],

$$\ln(z) = (z-1)\,{}_2F_1(1, 1; 2; 1-z), \tag{54}$$

utilizing this relation and substituting (54), the resulting expression in (50) and (51) can be rewritten as

$$\mathcal{I}_1 = c_1\rho_s \int_0^{\infty} t^{a+2} \exp\left(-\frac{t}{b}\right) {}_2F_1\left(1, 1; 2; -c_1\rho_s t^2\right)\mathrm{dt} \tag{55}$$

and

$$\mathcal{I}_2 = c_2\rho_s \int_0^{\infty} t^{a+2} \exp\left(-\frac{t}{b}\right) {}_2F_1\left(1, 1; 2; -c_2\rho_s t^2\right)\mathrm{dt}. \tag{56}$$

Using [37, eq. (44)] for solving the above equations, i.e., (55) and (56), $\mathcal{I}_1$ and $\mathcal{I}_2$ can be expressed as (57) and (58) respectively shown at the bottom of the next page.

So by utilizing (57) and (58), the closed-form expression for the SE of the IRS-assisted wireless system can be expressed as in (59), as shown at the bottom of the next page.

Further, it can be noted here that for the case of ideal transceiver i.e., the HPA is linear with unit gain, $\alpha^2 = 1$, and zero distortion noise, $\kappa_\delta^2 = 0$, and similarly the receiver is also linear, $\kappa_d^2 = 0$. Thus, from (53), $c_1 = 1$ and $c_2 = 0$, and substituting these into (57), the SE for ideal transceiver case can easily be evaluated.

1) SPECIAL CASE ($M = 1$)

For the special case, when the transmit SNR ρ is very high, For the special case of $M = 1$, the SE as defined in (46) can be rewritten as

$$SE = \int_0^\infty \log_2\left(1 + \frac{\alpha^2 t^2 \rho_s}{(\kappa_\delta^2 + \kappa_d^2)t^2\rho_s + 1}\right) f_{\mathcal{G}}^s(t)\mathrm{d}t. \quad (60)$$

or equivalently by substituting $f_{\mathcal{G}}^s(t)$ from (33)

$$SE = \int_0^\infty t \log_2\left(1 + \frac{\alpha^2 t^2 \rho_s}{(\kappa_\delta^2 + \kappa_d^2)t^2\rho_s + 1}\right) K_0(t)\mathrm{d}t. \quad (61)$$

After some mathematical manipulation, (61) can be rewritten as

$$SE = \frac{1}{\ln(2)} \int_0^\infty t\Big\{\ln\Big(1 + c_1 t^2 \rho_s\Big) - \ln\Big(1 + c_2 t^2 \rho_s\Big)\Big\} K_0(t)\mathrm{d}t, \quad (62)$$

or equivalently

$$SE = \frac{1}{\ln(2)}\{\mathcal{I}_3 - \mathcal{I}_4\}, \quad (63)$$

where

$$\mathcal{I}_3 = \int_0^\infty t \ln\Big(1 + c_1 \rho_s t^2\Big) K_0(t)\mathrm{d}t, \quad (64)$$

and

$$\mathcal{I}_4 = \int_0^\infty t \ln\Big(1 + c_2 \rho_s t^2\Big) K_0(t)\mathrm{d}t, \quad (65)$$

with $c_2 = \kappa_\delta^2 + \kappa_d^2$ and $c_1 = \alpha^2 + c_2$.

Now by utilizing the below relation [51, 03.04.26.0009.01],

$$K_v(\sqrt{z}) = \frac{1}{2} G_{0,2}^{2,0}\left(\frac{z}{4} \Big| \frac{v}{2}, \frac{-v}{2}\right) \quad (66)$$

$$\begin{aligned}
\mathcal{I}_1 = {} & \Big\{2b^{a+1}(a-1)\Big\}\Gamma(a)c_1\rho_s \ln\big(b\sqrt{c_1\rho_s}\big) + 2(a-1)b^{a+1}\Gamma(a)F_0(3+a) \\
& - \frac{\pi}{(2+a)(bc_1\rho_s)^{\frac{a}{2}+1}} \csc\Big(\frac{a\pi}{2}\Big)\, {}_1F_2\Big(1 + \frac{a}{2}; \frac{3}{2}, 2 + \frac{a}{2}, -\frac{1}{4b^2c_1\rho_s}\Big) \\
& - \frac{\pi}{(a+1)(c_1\rho_s)^{\frac{a+1}{2}}} \sec\Big(\frac{a\pi}{2}\Big)\, {}_1F_2\Big(\frac{a+1}{2}; \frac{1}{2}, \frac{a+3}{2}, -\frac{1}{4b^2c_1\rho_s}\Big) \\
& + ab^{a+1}\Gamma(a)\, {}_2F_3\Big(1, 1; 2, \frac{1-a}{2}, \frac{3-a}{2}, -\frac{1}{4b^2c_1\rho_s}\Big)
\end{aligned} \quad (57)$$

$$\begin{aligned}
\mathcal{I}_2 = {} & \Big\{2b^{a+1}(a-1)\Big\}\Gamma(a)c_2\rho_s \ln\big(b\sqrt{c_2\rho_s}\big) + 2(a-1)b^{a+1}\Gamma(a)F_0(3+a) \\
& - \frac{\pi}{(2+a)(bc_2\rho_s)^{\frac{a}{2}+1}} \csc\Big(\frac{a\pi}{2}\Big)\, {}_1F_2\Big(1 + \frac{a}{2}; \frac{3}{2}, 2 + \frac{a}{2}, -\frac{1}{4b^2c_2\rho_s}\Big) \\
& - \frac{\pi}{(a+1)(c_2\rho_s)^{\frac{a+1}{2}}} \sec\Big(\frac{a\pi}{2}\Big)\, {}_1F_2\Big(\frac{a+1}{2}; \frac{1}{2}, \frac{a+3}{2}, -\frac{1}{4b^2c_2\rho_s}\Big) \\
& + ab^{a+1}\Gamma(a)\, {}_2F_3\Big(1, 1; 2, \frac{1-a}{2}, -\frac{3-a}{2}, -\frac{1}{4b^2c_2\rho_s}\Big)
\end{aligned} \quad (58)$$

$$\begin{aligned}
SE = {} & (a-1)\frac{\Gamma(a)}{\Gamma(a+1)}\Big\{c_1\rho_s \log_2\Big(b^2c_1\rho_s\Big) - c_2\rho_s \log_2\Big(b^2c_2\rho_s\Big)\Big\} \\
& + \frac{\pi}{(2+a)b^{a+2}\ln(2)\,\Gamma(a+1)} \csc\Big(\frac{a\pi}{2}\Big)\Big\{\frac{1}{(c_2\rho_s)^{\frac{a}{2}+1}}\, {}_1F_2\Big(1 + \frac{a}{2}; \frac{3}{2}, 2 + \frac{a}{2}, -\frac{1}{4b^2c_2\rho_s}\Big) \\
& \qquad - \frac{1}{(c_1\rho_s)^{\frac{a}{2}+1}}\, {}_1F_2\Big(1 + \frac{a}{2}; \frac{3}{2}, 2 + \frac{a}{2}, -\frac{1}{4b^2c_1\rho_s}\Big)\Big\} \\
& + \frac{\pi}{(a+1)b^{a+1}\ln(2)\,\Gamma(a+1)} \sec\Big(\frac{a\pi}{2}\Big)\Big\{\frac{1}{(c_2\rho_s)^{\frac{a+1}{2}}}\, {}_1F_2\Big(\frac{a+1}{2}; \frac{1}{2}, \frac{a+3}{2}, -\frac{1}{4b^2c_2\rho_s}\Big) \\
& \qquad - \frac{1}{(c_1\rho_s)^{\frac{a+1}{2}}}\, {}_1F_2\Big(\frac{a+1}{2}; \frac{1}{2}, \frac{a+3}{2}, -\frac{1}{4b^2c_1\rho_s}\Big)\Big\} \\
& + \frac{a}{\ln(2)}\frac{\Gamma(a)}{\Gamma(a+1)}\Big\{{}_2F_3\Big(1, 1; 2, \frac{1-a}{2}, -\frac{3-a}{2}, -\frac{1}{4b^2c_1\rho_s}\Big) - {}_2F_3\Big(1, 1; 2, \frac{1-a}{2}, -\frac{3-a}{2}, -\frac{1}{4b^2c_2\rho_s}\Big)\Big\}
\end{aligned} \quad (59)$$

and [52, eq. (17)]

$$ {}_2F_1(a,b,c,-z) = \frac{\Gamma(c)}{\Gamma(a)\Gamma(b)} G_{2,2}^{1,2}\left(z \,|\, \begin{matrix} 1-a, 1-b \\ 0, 1-c \end{matrix}\right) \quad (67) $$

and by using (54), $\mathcal{I}_3$ and $\mathcal{I}_4$ can be re-written as

$$ \mathcal{I}_3 = \frac{c_1\rho_s}{2} \int_0^\infty t^3 G_{2,2}^{1,2}\left(c_1\rho_s t^2 \,|\, \begin{matrix} 0, 0 \\ 0, -1 \end{matrix}\right) G_{0,2}^{2,0}\left(\frac{t^2}{4} |0, 0\right) \mathrm{d}t \quad (68) $$

and

$$ \mathcal{I}_4 = \frac{c_2\rho_s}{2} \int_0^\infty t^3 G_{2,2}^{1,2}\left(c_2\rho_s t^2 \,|\, \begin{matrix} 0, 0 \\ 0, -1 \end{matrix}\right) G_{0,2}^{2,0}\left(\frac{t^2}{4} |0, 0\right) \mathrm{d}t \quad (69) $$

Now utilizing [53, Ch. 2.3], (68) and (69) can be solved as

$$ \mathcal{I}_3 = \frac{1}{4c_1\rho_s} G_{1,3}^{3,1}\left(\frac{1}{4c_1\rho_s} \,|\, \begin{matrix} -1 \\ -1, -1, 0 \end{matrix}\right) \quad (70) $$

and

$$ \mathcal{I}_4 = \frac{1}{4c_2\rho_s} G_{1,3}^{3,1}\left(\frac{1}{4c_2\rho_s} \,|\, \begin{matrix} -1 \\ -1, -1, 0 \end{matrix}\right) \quad (71) $$

Thus, the SE for the special case of $M = 1$, as defined in (63), can now be expressed by using (70) and (71) as below

$$ SE = \frac{1}{4\ln(2)\rho_s} \left\{ \frac{1}{c_1} G_{1,3}^{3,1}\left(\frac{1}{4c_1\rho_s} \,|\, \begin{matrix} -1 \\ -1, -1, 0 \end{matrix}\right) - \frac{1}{c_2} G_{1,3}^{3,1}\left(\frac{1}{4c_2\rho_s} \,|\, \begin{matrix} -1 \\ -1, -1, 0 \end{matrix}\right) \right\}. \quad (72) $$

2) SPECIAL CASE (LARGE *M*)

For the special case when the number of REs in the IRS is quite large i.e., $M >> 1$, the SE can be approximated as below.

From (46), the SE is defined as:

$$ SE = \int_0^\infty \log_2\left\{1 + \frac{\alpha^2 t^2}{\left(\kappa_\delta^2 + \kappa_d^2\right)t^2 + \frac{1}{\rho_s}}\right\} f_{\mathcal{G}}(t)\mathrm{d}t, \quad (73) $$

now when M is large, the value of t^2 is large and thus $(\kappa_\delta^2 + \kappa_d^2)t^2 >> \frac{1}{\rho_s}$. So, in (73), $\frac{1}{\rho_s}$ can be neglected in the denominator.

Thus, after some mathematical manipulation and simplification, the SE for the special case when M is large can be expressed as

$$ \begin{aligned} SE &= \int_0^\infty \log_2\left\{1 + \frac{\alpha^2 t^2}{\left(\kappa_\delta^2 + \kappa_d^2\right)t^2}\right\} f_{\mathcal{G}}(t)\mathrm{d}t, \\ &= \log_2\left\{1 + \frac{\alpha^2}{\left(\kappa_\delta^2 + \kappa_d^2\right)}\right\} \int_0^\infty f_{\mathcal{G}}(t)\mathrm{d}t, \\ &= \log_2\left\{1 + \frac{\alpha^2}{\left(\kappa_\delta^2 + \kappa_d^2\right)}\right\}. \end{aligned} \quad (74) $$

3) HIGH SNR APPROXIMATION

For the special case, when ρ_s is very large i.e., $\rho_s \to \infty$, from (46), the SE can be defined as:

$$ \lim_{\rho_s\to\infty} SE = \int_0^\infty \log_2\left\{1 + \frac{\alpha^2 t^2}{\left(\kappa_\delta^2+\kappa_d^2\right)t^2 + \frac{1}{\rho_s}}\right\} f_{\mathcal{G}}(t)\mathrm{d}t. \quad (75) $$

Now, utilizing the fact that $\frac{1}{\rho_s} \to 0$ as $\rho_s \to \infty$, we can rewrite the above as

$$ \lim_{\rho_s\to\infty} SE = \log_2\left\{1 + \frac{\alpha^2}{\left(\kappa_\delta^2 + \kappa_d^2\right)}\right\} \int_0^\infty f_{\mathcal{G}}(t)\mathrm{d}t, \quad (76) $$

or equivalently

$$ \lim_{\rho_s\to\infty} SE = \log_2\left\{1 + \frac{\alpha^2}{\left(\kappa_\delta^2 + \kappa_d^2\right)}\right\}. \quad (77) $$

From (74) and (77), it can be observed that for the case when the transmit SNR is very high or the number of REs is large, the SE saturates. Additionally, the SE can not be further enhanced either by increasing the transmit SNR or by increasing the number of REs. This is in contrast with the conventional case where the SE can be enhanced through increase in the transmit SNR. Further, for the case when the number of reflecting elements is larger, the SE saturates even for mild transit SNR. It may be noted here that, the approximation in (77) is the upper bound of SE for high SNR regime.

C. ENERGY EFFICIENCY (EE)

The EE of the IRS-assisted wireless system can be defined in terms of bits/Joule/Hz as the ratio of the SE and the total power consumed [54],

$$ EE = \frac{SE}{P_{tot}}, \quad (78) $$

where P_{tot} represents the sum of power consumed in transmission and the circuitry at the source, IRS and the destination.

Now the power consumption at the source comprises of the P_s, i.e., the source transmit power, P_{hpa}^S, i.e., the power consumed at the HPA, and P_c^S, i.e., the power required for the operation of other circuit components (excluding the power consumed at HPA).[4] The power consumed at the HPA can be modelled as $P_{hpa}^S = \beta P_s$, where $\beta = \frac{1}{\omega}$ and ω is the drain efficiency of HPA. Therefore, the total power consumption at the source can be written as

$$ P_{tot}^S = (1+\beta)P_s + P_c^S. \quad (79) $$

Similarly the power consumed at the destination can be written as

$$ P_{tot}^D = P_c^D, \quad (80) $$

where P_c^D is the power consumed at the destination circuitry. Since the IRS is equipped with multiple REs, for the ease

4. The other circuit power accounts for the power consumed by other blocks such as mixer, a digital-to-analog converter, frequency synthesizer.

TABLE 4. Simulation parameters.

Parameter	Simulation Values
Circuit Power	P_c^S=10 dBm, P_c^D=10 dBm [20]
IRS Power Consumption	P_c^{IRS} = 10 dBm [20]
Variance of AWGN Noise	$\sigma^2 = 1$
Variance of Channel Elements h_i, g_i	1 [37]
HPA Power Consumption Factor	β = 1.25 [54]

of exposition and without losing any generality, we assume that the power consumed by each of the RE is identical [20]. So, the power consumed at the IRS can be expressed as

$$P_{tot}^{IRS} = MP_c^{IRS}, \tag{81}$$

where P_c^{IRS} is the circuit power consumption at each RE of the IRS.

After taking into account the above, the EE in (78) can be expressed as

$$EE = \frac{SE}{(1+\beta)P_s + P_c^S + MP_{IRS} + P_c^D} \tag{82}$$

From (82), it can be observed that increasing M increases the power consumption linearly, whereas the SE increases logarithmically with respect to M. Thus, the overall impact will be a compound effect of both, where the EE increases initially with increasing M, but afterward the EE decreases. This has also been verified through simulation results in the next section.

IV. SIMULATION RESULTS

In this section, the theoretical framework provided in Section III is verified through simulations. The simulation results demonstrate the detrimental impact of hardware imperfections on IRS-assisted wireless systems. The main simulation parameters are summarized in Table 4.

A. OUTAGE

Fig. 3 shows the outage probability as a function of transmit SNR (ρ_s) for different values of M and ρ_{th}, where ρ_{th} ($\rho_{th} = 2^{R_{th}} - 1$) is the SNR threshold corresponding to the rate threshold R_{th}. From Fig. 3, the following observations can be made: a) increasing the number of REs significantly improves the outage probability, as can be seen from the plot for $M = 1$, 10 and 50, b) increasing ρ_{th}, reduces the outage probability as can be observed from the plot for $\rho_{th} = 0$, 5 and 10 dB, and c) increasing the transmit SNR results in a considerable change in outage performance when the number of reflecting elements is large. For instance, it can be viewed from here that for $M = 10$ at $\rho_{th} = 5$ dB, the outage probability reduces drastically from 10^{-1} to 10^{-7} on increasing the transmit SNR by 10 dB.

Fig. 4 shows the impact caused by the level of distortion noise on the performance of outage probability. A significant impact of κ here ($\kappa = \kappa_d$, can be observed on the outage probability of the IRS-assisted wireless system. Specifically,

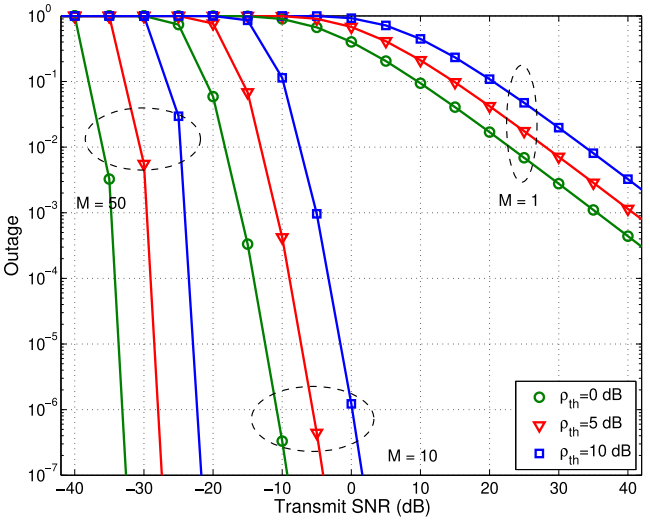

FIGURE 3. Analytical (lines) and simulation (marker points) shows the outage probability with respect to transmit SNR for varying number of reflecting elements and SNR threshold, at $\kappa = 0.1$.

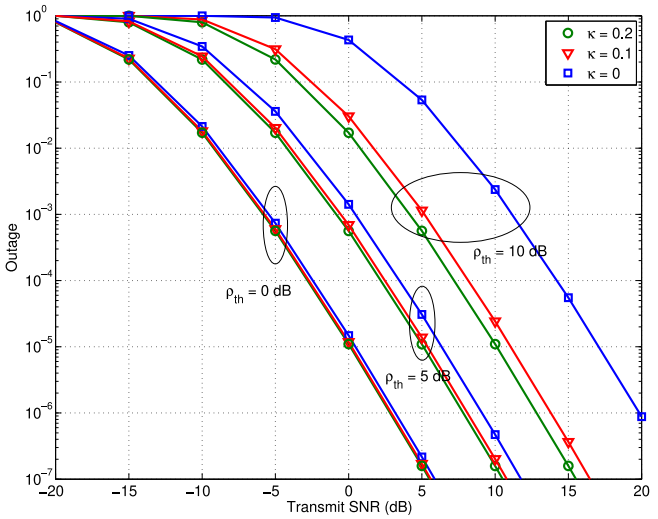

FIGURE 4. Analytical (lines) and simulation (marker points) shows the outage probability with respect to transmit SNR for various SNR threshold and distortion noise level, at $M = 10$.

the impact of distortion is more significant for higher SNR threshold, i.e., $\rho_{th} = 10$ dB. Further, for a lower SNR threshold, the outage probability is not significantly affected by the level of distortion noise. This is due to the fact that the lower SNR threshold corresponds to very low transmit SNR, where the contribution of white Gaussian noise is much more significant than the distortion noise. Moreover, increasing the transmit SNR improves the outage probability, which is quite obvious and intuitive as well.

B. SE AND EE

Fig. 5 shows the impact of HPA nonlinearity on the SE and EE of the IRS-assisted wireless system. It can be observed that the SE saturates with increasing transmit SNR.

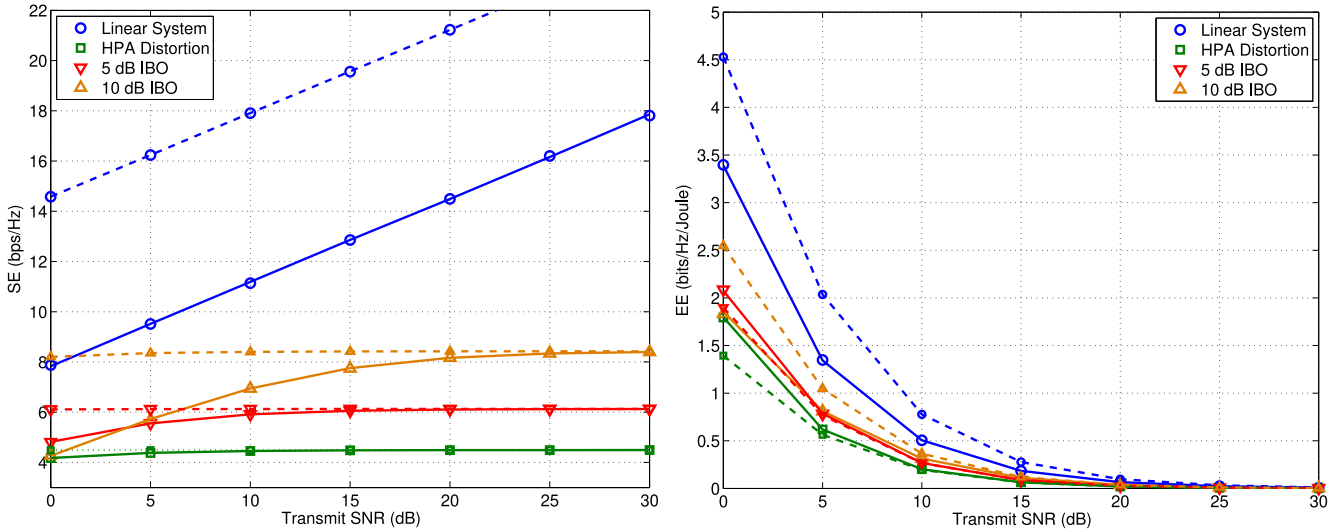

(a) SE (b) EE

FIGURE 5. **Analytical (lines) and simulation (marker points) results of SE and EE with respect to transmit SNR for different IBOs, solid and dashed lines represent M = 10 and 100 respectively.**

Further, the SE can be improved by operating HPA in the back-off region, which shifts the HPA operating point towards the linear region. It can also be observed here that when the number of REs increases, the SE saturates for lower transmit SNR, as can be seen from Fig. 5(a). Thus, it can be noted that in a nonlinear IRS-assisted wireless system with large M, the SE can not be increased by transmitting more power; however, it can be increased by mitigating the nonlinear distortion through operating the HPA with back-off. Further, operating the HPA in the back-off region reduces the power efficiency of HPA, which consequently impacts the overall EE of the system. Thus, there is a trade-off with respect to input back-off, increasing the IBO improves the SE at the cost of EE of the system.

Fig. 5(b) shows the EE for the IRS-assisted wireless system impaired by a nonlinear HPA. As discussed earlier as well, the EE reduces with increasing the transmit SNR. Further, it can also be observed that operating in the back-off improves the EE, which is due to the enhancement in the SE. Also, when the number of REs is increased, the EE further reduces; this is due to the fact that the SE is saturated, whereas the power consumption at the IRS is increasing. Moreover, it can be observed that increasing the number of REs improves the EE of a nonlinear system when there is sufficient back-off.

Fig. 6 shows the impact of HPA nonlinearity on the SE and EE of the IRS-assisted wireless system with respect to increasing the number of REs. Fig. 6(a) shows the SE with respect to the number of IRS REs, where it can be observed that for a nonlinear system, the SE saturates with the increase in the number of REs. Further, for large M, the SE saturates at even lower SNR. Thus either by increasing the transmit power or by increasing the number of REs, the SE saturates, and no further gain can be achieved. However, if the nonlinear distortion impact is reduced by operating in back-off, SE increases with the number of REs. Fig. 6(b) shows the EE of IRS assisted system with respect to increasing the number of REs. As evident from the result, the EE saturates with the increase in M. Further, for the higher transmit SNR, the EE starts decreasing with increase in M. Also, it can be noted here that the linear system is the most energy-efficient which is quite intuitive. The nonlinear HPA reduces the EE as can be observed from Fig. 6(b). However, operating the HPA with back-off improves the EE of IRS-assisted system.

Fig. 7(a) and (b) shows the SE and the EE of the IRS-assisted wireless system with respect to the transmit SNR, respectively. It can be observed from Fig. 7(a) that SE increases initially with the transmit power; however, it saturates at higher transmit power. It can be noted that after saturation, the SE can not be enhanced by increasing the transmit power. Further, for a fixed transmit SNR, the SE increases when the number of REs increases; however, at a higher transmit SNR, the SE saturates and it can not be improved by increasing the number of REs. Further, it is noted that as the number of REs increases, SE saturates at lower transmit power. As a consequence, it can be inferred that the distortion noise due to hardware impairments severely limits the SE of the IRS-assisted wireless system.

Fig. 7(b) shows the corresponding EE, where the EE reduces as the transmit power increase, which is quite obvious. It also shows that EE increases with the number of REs, but for a very large number of REs, the EE again decreases. It is interesting to note that increasing the number of REs does not always guarantee an increase in the EE. This can be due to the fact that increasing the number of REs also increases the circuit power consumption, whereas the SE

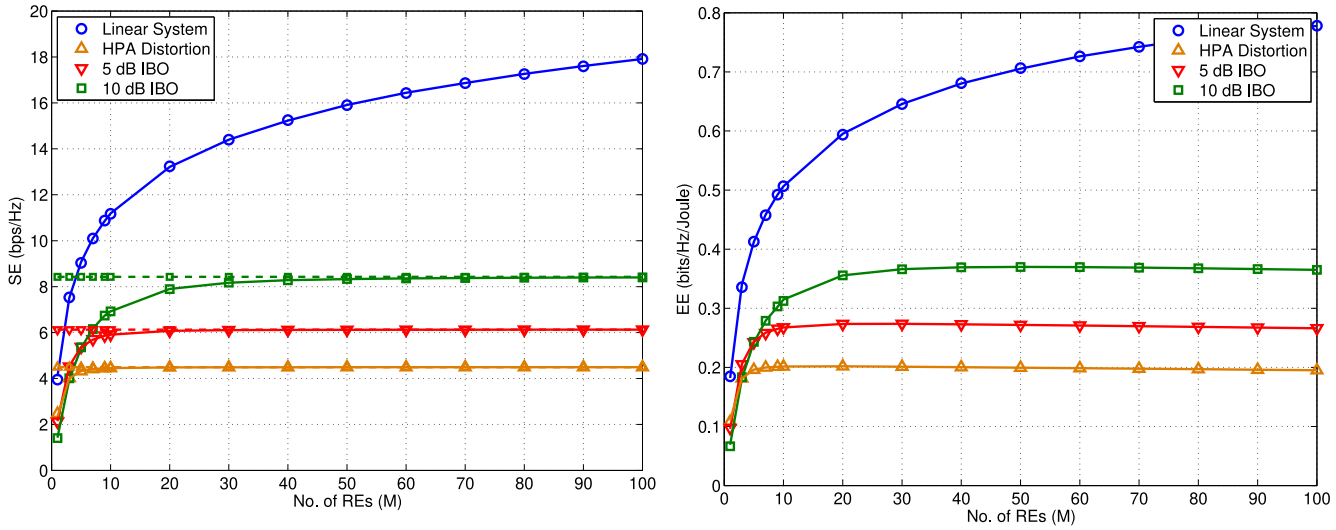

(a) SE (b) EE

FIGURE 6. Analytical (lines) and simulation (marker points) results of SE and EE with respect to M for different IBOs, solid and dashed lines represent SNR = 10 and 20 dB respectively.

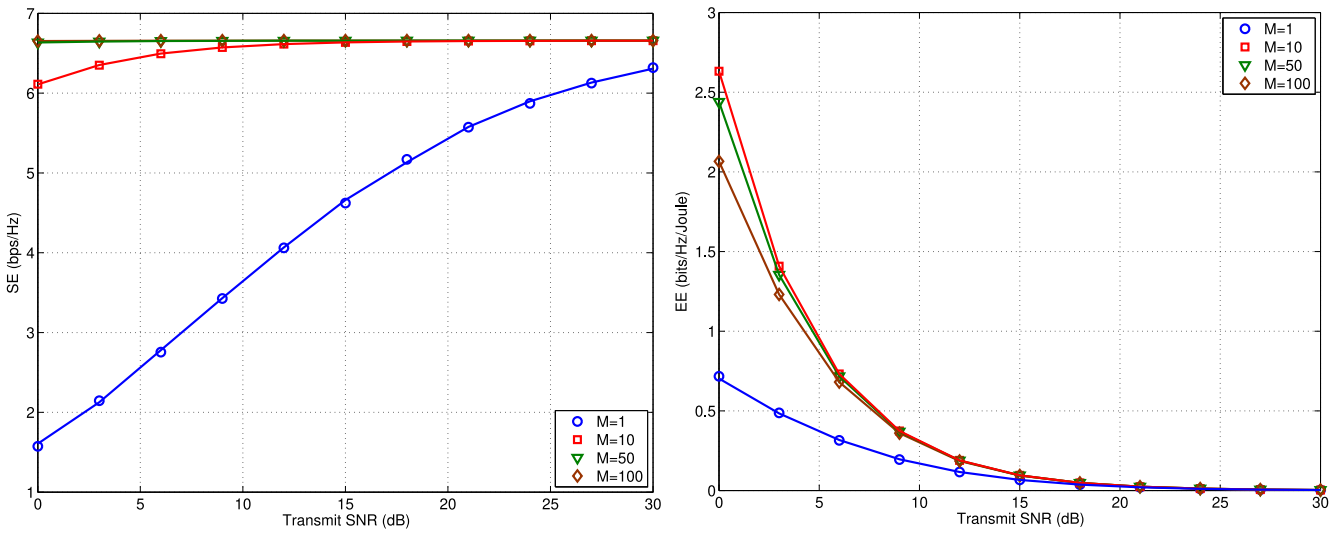

(a) SE (b) EE

FIGURE 7. Analytical (solid lines) and simulation (marker points) results of SE and EE with respect to transmit SNR for varying number of reflecting elements (M), assuming $\kappa = 0.1$.

saturates after an initial increment. Thus this compounding impact results in a decrease in the EE for a large number of REs. This can also be observed analytically from (82).

Fig. 8 shows the impact of the varying distortion noise level on the SE and the EE of the IRS-assisted wireless system. Fig. 8(a) shows the SE with respect to transmit power level and varying distortion noise level. The result shows that the SE reduces with a increase in the level of distortion noise. Further, for each distortion noise level, the SE saturates as the transmit SNR is increased. As a performance benchmark, the SE without distortion, i.e., for an ideal linear IRS system, is also plotted.

Fig. 8(b) shows the EE with respect to the transmit power level. As discussed earlier, increasing the transmit power reduces the EE of the system. Further, as can be seen from above, EE degrades with an increase in the level of distortion noise, which is due to the fact that increasing distortion noise level reduces the SE; consequently, the EE also worsens accordingly.

Fig. 9 shows the joint impact of the HPA nonlinearity at the source and hardware distortion at the destination. Fig. 9(a) shows the SE of the IRS-assisted wireless system, whereas Fig. 9(b) shows the EE. As evident from Fig. 9(a), the HPA nonlinearity is more significant and detrimental than the hardware distortion of the destination. Moreover, the joint impact of source and destination nonlinearity further degrades the SE of the IRS-assisted system. However, the HPA nonlinearity can be alleviated by operating the HPA in

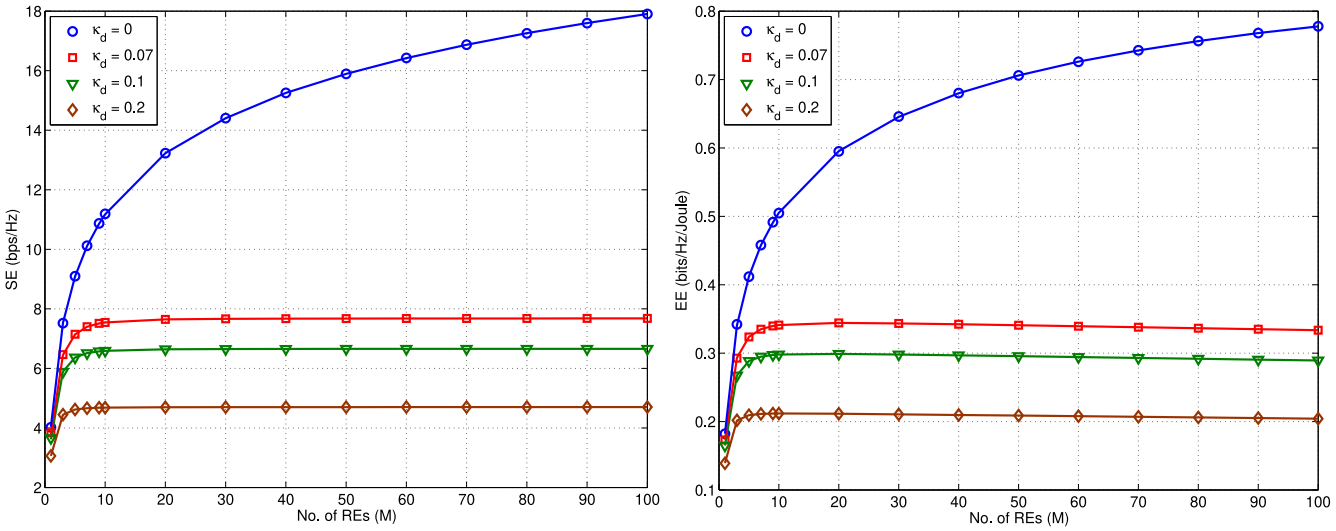

(a) SE (b) EE

FIGURE 8. Analytical (solid lines) and simulation (marker points) results of SE and EE with respect to the number of reflecting elements for various distortion noise level (κ), assuming transmit SNR, $\rho_S = 10$ dB.

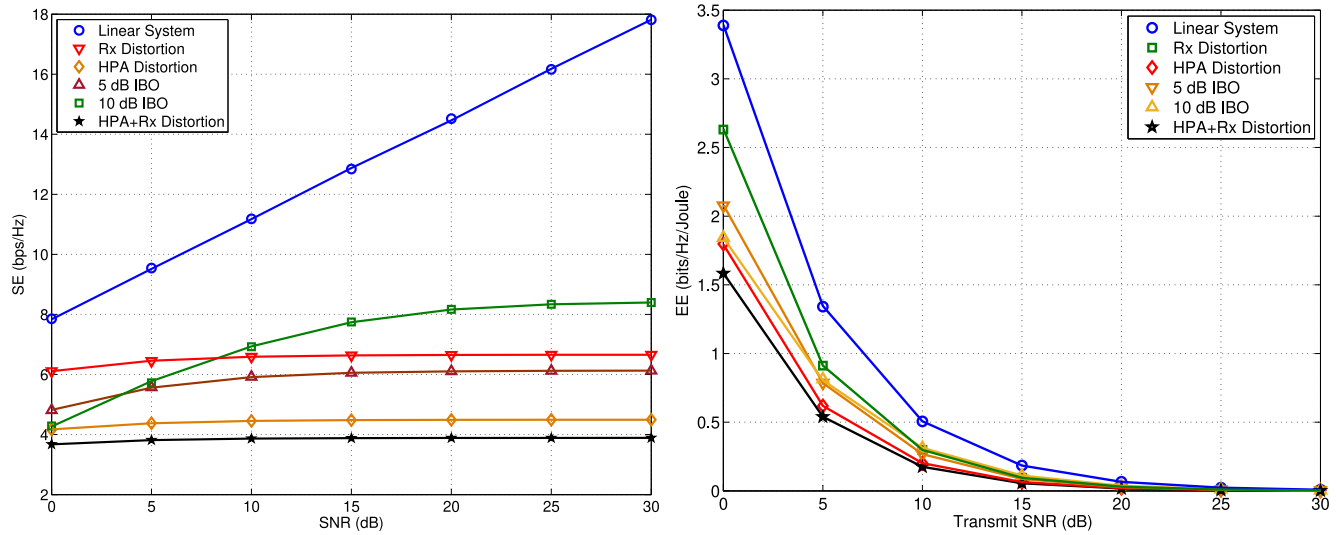

(a) SE (b) EE

FIGURE 9. Analytical (lines) and simulation (marker points) results of SE and EE with respect to transmit SNR for different IBOs at $M = 10$, assuming $\kappa = 0.1$.

the back-off region, although it reduces the HPA efficiency, thereby impacting the EE of the system. It can be seen from Fig. 9(a) that increasing the transmit SNR saturates the SE performance irrespective of the distortion that occurs due to destination hardware impairment or source HPA nonlinearity. However, the saturation level of SE can be increased by large input back-off. Similar observations can be made on the EE performance, as evident from Fig. 9(b). Additionally, Table 5 summarize the comparison of ideal and non-ideal hardware based IRS-assisted wireless transmission system.

It can be inferred that the linear system has the best EE, whereas the joint source HPA nonlinearity and destination hardware impairment has the worse EE. Further, it can also be concluded from the above result, that the HPA is the major source of nonlinear distortion. Although, the impact of HPA distortion can be mitigated through operating in the back-off region. However, operating HPA in the back-off

TABLE 5. Evaluation matrix.

Simulation Parameter	Ideal Transceiver		Non-Ideal Transceiver	
	SE	EE	SE	EE
$M = 1,\ \rho_s = 10$ dB	4.14	0.185	2.12	0.099
$M = 1,\ \rho_s = 20$ dB	33.64	0.152	3.89	0.018
$M = 10,\ \rho_s = 10$ dB	11.18	0.507	3.86	0.175
$M = 10,\ \rho_s = 20$ dB	41.12	0.187	3.89	0.018
$M = 100,\ \rho_s = 10$ dB	17.90	0.777	3.89	0.169
$M = 100,\ \rho_s = 20$ dB	47.80	0.216	3.89	0.018

reduces the operating efficiency and consequently, there is trade-off between the SE and EE with respect to HPA back-off. Thus as evident from the above, the non-ideal transceiver significantly impact the performance of IRS-assisted wireless system. So, these contributions can not be neglected in a practical deployment of IRS based wireless systems.

V. CONCLUSION

This work considers the impact of transceiver impairment on the performance of IRS-assisted wireless systems. Specifically, we have analyzed the SE, EE and outage probability by deriving the closed-form expressions. The HPA nonlinearity at the source has been characterized through AM/AM and AM/PM distortions, whereas a generalized additive Gaussian distortion model has been considered to characterize the hardware imperfections at the destination. The results show that the detrimental impact of hardware imperfection cannot be neglected while analyzing the performance of these systems. It can also be observed that after a particular SNR, SE saturates, and any further gain can neither be realized by increasing the number of REs nor by enhancing the transmit power.

ACKNOWLEDGMENT

The authors would like to thank the anonymous reviewers for their constructive comments and criticism.

REFERENCES

[1] M. Xiao *et al.*, "Millimeter wave communications for future mobile networks," *IEEE J. Sel. Areas Commun.*, vol. 35, no. 9, pp. 1909–1935, Sep. 2017.

[2] M. A. Habibi, M. Nasimi, B. Han, and H. D. Schotten, "A comprehensive survey of RAN architectures toward 5G mobile communication system," *IEEE Access*, vol. 7, pp. 70371–70421, 2019.

[3] M. Shafi *et al.*, "5G: A tutorial overview of standards, trials, challenges, deployment, and practice," *IEEE J. Sel. Areas Commun.*, vol. 35, no. 6, pp. 1201–1221, Jun. 2017.

[4] I. F. Akyildiz, S. Nie, S.-C. Lin, and M. Chandrasekaran, "5G roadmap: 10 key enabling technologies," *Comput. Netw.*, vol. 106, pp. 17–48, Sep. 2016.

[5] L. Lu, G. Y. Li, A. L. Swindlehurst, A. Ashikhmin, and R. Zhang, "An overview of massive MIMO: Benefits and challenges," *IEEE J. Sel. Topics Signal Process.*, vol. 8, no. 5, pp. 742–758, Oct. 2014.

[6] Q. Wu, G. Y. Li, W. Chen, D. W. K. Ng, and R. Schober, "An overview of sustainable green 5G networks," *IEEE Wireless Commun.*, vol. 24, no. 4, pp. 72–80, Aug. 2017.

[7] R. Mahapatra, Y. Nijsure, G. Kaddoum, N. U. Hassan, and C. Yuen, "Energy efficiency tradeoff mechanism towards wireless green communication: A survey," *IEEE Commun. Surveys Tuts.*, vol. 18, no. 1, pp. 686–705, 1st Quart., 2016.

[8] M. H. N. Shaikh, V. A. Bohara, P. Aggarwal, and A. Srivastava, "Energy efficiency evaluation for downlink full-duplex nonlinear MU-MIMO-OFDM system with self-energy recycling," *IEEE Syst. J.*, vol. 14, no. 3, pp. 3313–3324, Sep. 2020.

[9] S. Buzzi, I. Chih-Lin, T. E. Klein, H. V. Poor, C. Yang, and A. Zappone, "A survey of energy-efficient techniques for 5G networks and challenges ahead," *IEEE J. Sel. Areas Commun.*, vol. 34, no. 4, pp. 697–709, Apr. 2016.

[10] E. Björnson, J. Hoydis, M. Kountouris, and M. Debbah, "Massive MIMO systems with non-ideal hardware: Energy efficiency, estimation, and capacity limits," *IEEE Trans. Inf. Theory*, vol. 60, no. 11, pp. 7112–7139, Nov. 2014.

[11] X. Gao, O. Edfors, F. Tufvesson, and E. G. Larsson, "Massive MIMO in real propagation environments: Do all antennas contribute equally?" *IEEE Trans. Commun.*, vol. 63, no. 11, pp. 3917–3928, Nov. 2015.

[12] S. Hu, F. Rusek, and O. Edfors, "Beyond massive MIMO: The potential of data transmission with large intelligent surfaces," *IEEE Trans. Signal Process.*, vol. 66, no. 10, pp. 2746–2758, May 2018.

[13] G. Gui, M. Liu, F. Tang, N. Kato, and F. Adachi, "6G: Opening new horizons for integration of comfort, security and intelligence," *IEEE Wireless Commun.*, vol. 27, no. 5, pp. 126–132, Oct. 2020.

[14] S. Dang, O. Amin, B. Shihada, and M.-S. Alouini, "What should 6G be?" *Nat. Electron.*, vol. 3, no. 1, pp. 20–29, 2020.

[15] M. D. Renzo *et al.*, "Smart radio environments empowered by reconfigurable ai meta-surfaces: An idea whose time has come," *EURASIP J. Wireless Commun. Netw.*, no. 1, pp. 1–20, 2019.

[16] L. Dai *et al.*, "Reconfigurable intelligent surface-based wireless communications: Antenna design, prototyping, and experimental results," *IEEE Access*, vol. 8, pp. 45913–45923, 2020.

[17] C. Liaskos, S. Nie, A. Tsioliaridou, A. Pitsillides, S. Ioannidis, and I. Akyildiz, "A new wireless communication paradigm through software-controlled metasurfaces," *IEEE Commun. Mag.*, vol. 56, no. 9, pp. 162–169, Sep. 2018.

[18] Y. Yang, B. Zheng, S. Zhang, and R. Zhang, "Intelligent reflecting surface meets OFDM: Protocol design and rate maximization," *IEEE Trans. Commun.*, vol. 68, no. 7, pp. 4522–4535, Jul. 2020.

[19] C. Huang, G. C. Alexandropoulos, A. Zappone, M. Debbah, and C. Yuen, "Energy efficient multi-user MISO communication using low resolution large intelligent surfaces," in *Proc. IEEE GLOBECOM Workshops*, 2018, pp. 1–6.

[20] C. Huang, A. Zappone, G. C. Alexandropoulos, M. Debbah, and C. Yuen, "Reconfigurable intelligent surfaces for energy efficiency in wireless communication," *IEEE Trans. Wireless Commun.*, vol. 18, no. 8, pp. 4157–4170, Aug. 2019.

[21] E. Basar, M. D. Renzo, J. De Rosny, M. Debbah, M.-S. Alouini, and R. Zhang, "Wireless communications through reconfigurable intelligent surfaces," *IEEE Access*, vol. 7, pp. 116753–116773, 2019.

[22] H. Zhang, B. Di, L. Song, and Z. Han, "Reconfigurable intelligent surfaces assisted communications with limited phase shifts: How many phase shifts are enough?" *IEEE Trans. Veh. Technol.*, vol. 69, no. 4, pp. 4498–4502, Apr. 2020.

[23] M. Jung, W. Saad, Y. Jang, G. Kong, and S. Choi, "Reliability analysis of large intelligent surfaces (LISs): Rate distribution and outage probability," *IEEE Wireless Commun. Lett.*, vol. 8, no. 6, pp. 1662–1666, Dec. 2019.

[24] C. Huang, A. Zappone, M. Debbah, and C. Yuen, "Achievable rate maximization by passive intelligent mirrors," in *Proc. IEEE ICASSP*, 2018, pp. 3714–3718.

[25] E. Basar, "Transmission through large intelligent surfaces: A new frontier in wireless communications," in *Proc. EuCNC*, 2019, pp. 112–117.

[26] V. C. Thirumavalavan and T. S. Jayaraman, "BER analysis of reconfigurable intelligent surface assisted downlink power domain NOMA system," in *Proc. IEEE COMSNETS*, 2020, pp. 519–522.

[27] C. Pan *et al.*, "Intelligent reflecting surface aided MIMO broadcasting for simultaneous wireless information and power transfer," *IEEE J. Sel. Areas Commun.*, vol. 38, no. 8, pp. 1719–1734, Aug. 2020.

[28] B. Lyu, P. Ramezani, D. T. Hoang, S. Gong, Z. Yang, and A. Jamalipour, "Optimized energy and information relaying in self-sustainable IRS-empowered WPCN," *IEEE Trans. Commun.*, vol. 69, no. 1, pp. 619–633, Jan. 2021.

[29] E. Basar, "Reconfigurable intelligent surface-based index modulation: A new beyond MIMO paradigm for 6G," *IEEE Trans. Commun.*, vol. 68, no. 5, pp. 3187–3196, May 2020.

[30] Q. Wu and R. Zhang, "Beamforming optimization for intelligent reflecting surface with discrete phase shifts," in *Proc. IEEE ICASSP*, 2019, pp. 7830–7833.

[31] X. Yu, D. Xu, and R. Schober, "Enabling secure wireless communications via intelligent reflecting surfaces," in *Proc. IEEE GLOBECOM*, 2019, pp. 1–6.

[32] Y. Chen, Y. Wang, J. Zhang, and Z. Li, "Resource allocation for intelligent reflecting surface aided vehicular communication," *IEEE Trans. Veh. Technol.*, vol. 69, no. 10, pp. 12321–12326, Oct. 2020.

[33] M. D. Renzo *et al.*, "Smart radio environments empowered by reconfigurable intelligent surfaces: How it works, state of research, and the road ahead," *IEEE J. Sel. Areas Commun.*, vol. 38, no. 11, pp. 2450–2525, Nov. 2020.
[34] Q. Wu and R. Zhang, "Towards smart and reconfigurable environment: Intelligent reflecting surface aided wireless network," *IEEE Commun. Mag.*, vol. 58, no. 1, pp. 106–112, Jan. 2020.
[35] E. Björnson, Ö. Özdogan, and E. G. Larsson, "Intelligent reflecting surface versus decode-and-forward: How large surfaces are needed to beat relaying?" *IEEE Wireless Commun. Lett.*, vol. 9, no. 2, pp. 244–248, Feb. 2020.
[36] M. D. Renzo *et al.*, "Reconfigurable intelligent surfaces vs. relaying: Differences, similarities, and performance comparison," *IEEE Open J. Commun. Soc.*, vol. 1, pp. 798–807, 2020.
[37] A. A. Boulogeorgos and A. Alexiou, "Performance analysis of reconfigurable intelligent surface-assisted wireless systems and comparison with relaying," *IEEE Access*, vol. 8, pp. 94463–94483, 2020.
[38] A.-A. Boulogeorgos and A. Alexiou, "How much do hardware imperfections affect the performance of reconfigurable intelligent surface-assisted systems?" *IEEE Open J. Commun. Soc.*, vol. 1, pp. 1185–1195, 2020.
[39] A. Papazafeiropoulos, S. K. Sharma, T. Ratnarajah, and S. Chatzinotas, "Impact of residual additive transceiver hardware impairments on rayleigh-product MIMO channels with linear receivers: Exact and asymptotic analyses," *IEEE Trans. Commun.*, vol. 66, no. 1, pp. 105–118, Jan. 2018.
[40] J. Qi and S. Aissa, "Analysis and compensation of power amplifier nonlinearity in MIMO transmit diversity systems," *IEEE Trans. Veh. Technol.*, vol. 59, no. 6, pp. 2921–2931, Jul. 2010.
[41] V. A. Bohara and S. H. Ting, "Analytical performance of orthogonal frequency division multiplexing systems impaired by a non-linear high-power amplifier with memory," *IET Commun.*, vol. 3, no. 10, pp. 1659–1666, Oct. 2009.
[42] V. A. Bohara and S. H. Ting, "Analysis of OFDM signals in nonlinear high power amplifier with memory," in *Proc. IEEE ICC*, 2008, pp. 3653–3657.
[43] P. Aggarwal, A. Pradhan, and V. A. Bohara, "A downlink multiuser MIMO-OFDM system with nonideal oscillators and amplifiers: Characterization and performance analysis," *IEEE Syst. J.*, vol. 15, no. 1, pp. 715–726, Mar. 2021.
[44] H. E. Rowe, "Memoryless nonlinearities with Gaussian inputs: Elementary results," *Bell Syst. Tech. J.*, vol. 61, no. 7, pp. 1519–1525, Sep. 1982.
[45] E. Balti and M. Guizani, "Impact of non-linear high-power amplifiers on cooperative relaying systems," *IEEE Trans. Commun.*, vol. 65, no. 10, pp. 4163–4175, Oct. 2017.
[46] X. Yang, M. Matthaiou, J. Yang, C.-K. Wen, F. Gao, and S. Jin, "Hardware-constrained millimeter-wave systems for 5G: Challenges, opportunities, and solutions," *IEEE Commun. Mag.*, vol. 57, no. 1, pp. 44–50, Jan. 2019.
[47] E. Björnson, M. Matthaiou, and M. Debbah, "Massive MIMO systems with hardware-constrained base stations," in *Proc. IEEE ICASSP*, 2014, pp. 3142–3146.
[48] E. Björnson, A. Papadogiannis, M. Matthaiou, and M. Debbah, "On the impact of transceiver impairments on af relaying," in *Proc. IEEE ICASSP*, 2013, pp. 4948–4952.
[49] A.-A. A. Boulogeorgos, N. D. Chatzidiamantis, and G. K. Karagiannidis, "Energy detection spectrum sensing under RF imperfections," *IEEE Trans. Commun.*, vol. 64, no. 7, pp. 2754–2766, Jul. 2016.
[50] J. P. Hannah, "Identities for the gamma and hypergeometric functions: An overview from euler to the present," M.S. thesis, Sch. Math., Univ. Witwatersrand, Johannesburg, South Africa, 2013.
[51] *The Wolfram Functions Site*, Wolfram, Champaign, IL, USA, Dec. 2020.
[52] V. S. Adamchik and O. I. Marichev, "The algorithm for calculating integrals of hypergeometric type functions and its realization in reduce system," in *Proc. Int. Symp. Symbolic Algebraic Comput.*, 1990, pp. 212–224.
[53] A. Mathai, R. K. Saxena, and H. J. Haubold, *The H-Function: Theory and Applications*. New York, NY, USA: Springer-Verlag, 2010.
[54] M. H. N. Shaikh, V. A. Bohara, and A. Srivastava, "Performance analysis of a full-duplex MIMO decode-and-forward relay system with self-energy recycling," *IEEE Access*, vol. 8, pp. 226248–226266, 2020.

MOHD HAMZA NAIM SHAIKH (Graduate Student Member, IEEE) received the B.Tech. and M.Tech. degrees from Aligarh Muslim University, Aligarh, India, in 2014 and 2016, respectively. He is currently pursuing the Ph.D. degree with IIIT Delhi, Delhi, India. His research interests include next-generation communication technologies, such as FD radios, massive MIMO, RIS, and NOMA.

VIVEK ASHOK BOHARA (Senior Member, IEEE) received the Ph.D. degree from the School of EEE, Nanyang Technological University, Singapore, in 2011. From 2011 to 2013, he was a Postdoctoral Researcher (Marie Curie Fellowship) with ESIEE Paris, University Paris-East. He joined IIIT Delhi in 2013, where he is currently working as an Associate Professor. His research interests are towards next-generation communication technologies, such as device-to-device communication, carrier aggregation, and digital predistortion algorithms. He received the First Prize in National Instruments ASEAN Virtual Instrumentation Applications Contest in 2007 and 2010. He was also the recipient of the Best Poster Award at IEEE ANTS 2014 and IEEE COMSNETS 2015 and 2016 conferences.

ANAND SRIVASTAVA received the M.Tech. and Ph.D. degrees from the Indian Institute of Technology (IIT) Delhi, India, in 2002. Before joining IIIT Delhi in 2014, he was a Dean and a Professor with the School of Computing and Electrical Engineering, IIT Mandi, India from 2012 to 2014, and also has been an Adjunct Professor with IIT Delhi since 2008. Prior to this, he worked with Alcatel-Lucent- Bell Labs from 2009 to 2012, India and Center for Development of Telematics (CDOT), a Telecom Research Center of Government of India from 1989 to 2008. During his stint in CDOT for nearly two decades, he was responsible for the development of national-level projects for Indian Telecom in the areas of Telecom Security Systems, Network Management System, Intelligent Networks, Operations Support Systems, Access Networks (GPON), and Optical Technology based products. Majority of these projects were completed successfully and commercially deployed in the public network. He also carried out significant research work in the Photonics Research Lab, Nice, France, under the Indo-French Science and Technology Cooperation Program on Special optical fibers and fiber-based components for optical communications from 2007 to 2010. He was also closely involved with ITU-T, Geneva in Study Group 15 and represented India for various optical networking standards meetings. He has visited Aston University, U.K. four times from 2014 to 2016 as a Visiting Scholar under Erasmus Mundus EU program for carrying out research in optical wireless area. He has published several papers in peer-reviewed journals and conferences. His current research work is in the area of optical core and access networks, fiber-wireless (FiWi) architectures, visible light communications, optical signal processing, free space optical communications, and energy aware optical networks.

GOURAB GHATAK (Member, IEEE) received the master's degree from IIT Kanpur, India, and the Ph.D. degree with a thesis on multi-RAT 5G networks from Telecom ParisTech (ENST), France, in 2019. Prior to that, he was a DAAD Research Scholar with the Vodafone Chair Mobile Communications Systems, TU Dresden, Germany, from 2014 to 2015, where he worked on channel estimation schemes for GFDM. During his Ph.D., he was employed with CEA-LETI, Grenoble. He has been an Assistant Professor with IIIT Delhi, India, since January 2019. He is the Inventor of four patents and the authored several journals and conference publications. His research interests include stochastic geometry and machine learning for wireless communications. He has won the Best Paper Award from the 4th International Workshop on Smart Wireless Communications, 2017, Rome, Italy.